PERGAMON

International Journal of Heat and Mass Transfer 45 (2002) 3865–3873

International Journal of HEAT and MASS TRANSFER

www.elsevier.com/locate/ijhmt

Influence of coherent structures on mass transfer near stagnation region in agitated small tanks

L. Gbahoue, F. Barbeu, S. Martemianov *

Laboratoire d'Etudes Thermiques, UMR CNRS 6608, ESIP, 40 Avenue du Recteur Pineau, 86022 Poitiers Cedex, France

Received 20 November 2000; received in revised form 26 October 2001

Abstract

Electrochemical method is applied to study coherent structures in a complex three-dimensional flow generated by a rotating magnetic rod. In order to detect these structures, the power spectral density (PSD) analysis of the limiting diffusion current fluctuations is provided. This analysis reveals the existence of resonance frequencies when the probe is located in the very vicinity of the stirrer. The main resonance is related to the mechanical excitation frequency. The detailed analysis of the PSD curves points out some mechanisms of development of turbulence as sub-harmonics and non-linear interactions. For different locations of the probe and different angular rates of the stirrer Ω, a similarity of the energy repartition is obtained when the PSD is plotted versus the adimensional frequency f/Ω. Flow visualization by laser tomography is also provided and the local secondary flow past the electrode probe is sketched. The laser Doppler velocimetry (LDV) at a given location in a horizontal z-plane indicates a tornado wise mean flow structure.

1. Introduction

Electrochemical measurements are used to characterize the flow and the mass transfer in the vicinity of the stagnation region of a tornado wise flow supplied by a rotating magnetic rod. Such a device, as well as different types of turbines, is widely used in order to enhance heat and mass transfer in small chemical reactors. Flow stirring in batch reactors gives rise to a complex three-dimensional vortex structure. Many authors have investigated the influence of mixing on heat and mass transfer in agitated tanks, mainly with respect to mean characteristics. Some papers [1–4] deal with the bulk turbulence parameters: intensity, turbulent kinetic energy, local energy dissipation rate and energy spectra. Authors aimed in this way to determine the influence of turbulence on mixing performances as well as on mass transfer properties of a reactor. Data measurements were conducted with various techniques: constant temperature anemometer with a split-film probe [5], laser Doppler velocimetry (LDV) [3,4], 2D-LDV [1]. According to Wu et al. [4], fluctuations of the measured velocity in the vicinity of the impeller tip contain a large proportion of periodic components due to the periodic disturbance of the vortices generated by the impeller blades. Michelet et al. [1] determined the convection velocity and the scales of the turbulent structures on the base of space-time correlations. Ogawa and Mori [2] used electrochemical method to scale up industrial agitated tank by studying the size effect on the spectrum of turbulent energy. Khomchenko et al. [14–16] reported the electrochemical flow measurements in stirring electrochemical cell with complex geometry. The authors provided these studies in order to investigate the influence of turbulence on the kinetics of electrochemical processes. No particularities concerning the power spectral density of electrochemical current fluctuations were reported. Till to our knowledge, the use of electrochemical diagnostics for study of coherent structures in agitated tanks are rather scarcely known item. The present paper emphasizes the following points:

* Corresponding author.

E-mail address: martemianov@esip.univ-poitiers.fr (S. Martemianov).

0017-9310/02/$ - see front matter
PII: S0017-9310(02)00081-9

Nomenclature

A	electrode section area $A = \pi d^2/4$ (m^2)
b	diameter of the magnetic rod (m)
$\mathscr{D}$	diffusion coefficient (m^2 s^{-1})
d	diameter of circular microelectrode (m)
d_0	internal diameter of the reactor (m)
F	Faraday number $F = 96\,500$ (C mol^{-1})
$f_1 = f_{res}$	resonance frequency (Hz)
f_2	second independent frequency (Hz)
C	concentration of electroactive species (mol m^{-3})
C_0	concentration of electroactive species at the interface ($C_0 = 0$ for limiting diffusion current conditions) (mol m^{-3})
C_∞	bulk concentration of electroactive species (mol m^{-3})
I	limiting diffusion current (A)
i'	fluctuation of the limiting diffusion current (A)
$\bar{K}$	average mass transfer coefficient (m s^{-1})
L	length of the magnetic rod (m)
N	rotation rate of the magnetic rod (rps)
n	number of electrons transferred in the redox reaction
r	radial co-ordinate (m)
r_1, r_2, r_3	radial locations: $r_1/L = 0.48$; $r_2/L = 0.96$; $r_3/L = 1.44$ (m)
x, y	longitudinal and normal co-ordinate related to the electrode (m)
y_τ	length scale of the viscous layer $= \nu(\tau/\rho)^{-0.5}$ (m)
z_0	vertical distance from the bottom of the reactor $= 0.24L$ (m)

Dimensionless group

d^+	Microelectrode diameter scale $= d/y_\tau$
Sc	Schmidt number $= \nu/\mathscr{D}$
Sh	Sherwood number $= \bar{K}d/\mathscr{D} = d/\delta_N$

Greek symbols

Ω	angular rate (rad s^{-1})
δ_N	diffusion layer thickness (Nernst assumption) (m)
τ	longitudinal shear stress at the interface (Pa)
μ	dynamic viscosity (Pa s)
ν	kinematic viscosity $= \mu/\rho$ (m^2 s^{-1})

(i) *Sensitivity*. Can the electrochemical measurements be sensitive to coherent structures arising in complex three-dimensional turbulent flows?
(ii) *Turbulent mechanisms*. What kind of information concerning turbulent mechanisms in agitated tanks could be obtained by means of power spectral density (PSD) analysis of the limiting diffusion current fluctuations?

2. Experimental facility

2.1. Electrochemical method

Although formerly known in its principle [12,13], electrochemical method is more and more used for flow diagnostics [6–8]. The method is based on the limiting diffusion current measurements of fast oxydo-reduction electrochemical reactions. In our experiments we use a system of 0.005 M equimolar aqueous solution of $K_3Fe(CN)_6$ and $K_4Fe(CN)_6$, with a 0.3 M of K_2SO_4 as the supporting electrolyte. The Schmidt number for this electrochemical system is about 1360 at 298 K. The reaction at the cathode is then

$$Fe(CN)_6^{3-} + e \rightarrow Fe(CN)_6^{4-}$$

The limiting diffusion current is directly connected to mass flux at the cathode surface, so, the electrode works as a mass flux-meter.

Both mean and fluctuating current characteristics were measured. Data acquisition is supplied by a TEAC RD-125T digital recorder. The Fourier spectra are achieved by DIFA 100 software. The data acquisition frequency was 200 Hz for time duration of 10.24 s.

The study was carried out in a baffleless small reactor (Fig. 1) of $d_0 = 85$ mm internal diameter. The flow was generated by means of a magnetic rod ($b = 6$ mm in diameter and $L = 25$ mm in length) rotating at slow and moderate angular rates Ω. The aspect ratio is $d_0/L = 3.4$. The working electrode cathode was a platinum wire of 0.5 mm diameter flush mounted and electrically isolated in a 5 mm external diameter steel sheath (anode). This electrode system is directly submerged in the reactor till the cathode reaches $z_0 = 8$ mm ($z_0/b = 1.33$) from the bottom. Then the probe can be moved in different locations in the z_0 plane along a radius from the reactor vertical axis. Four different locations were studied ($2r_1/L \approx 0$; ≈ 0.48; ≈ 0.96; ≈ 1.44), (Fig. 1). It is to be noticed that for the locations 1 and 2, the cathode is very close to the rotating rod. It is not the case for the two other locations of the probe.

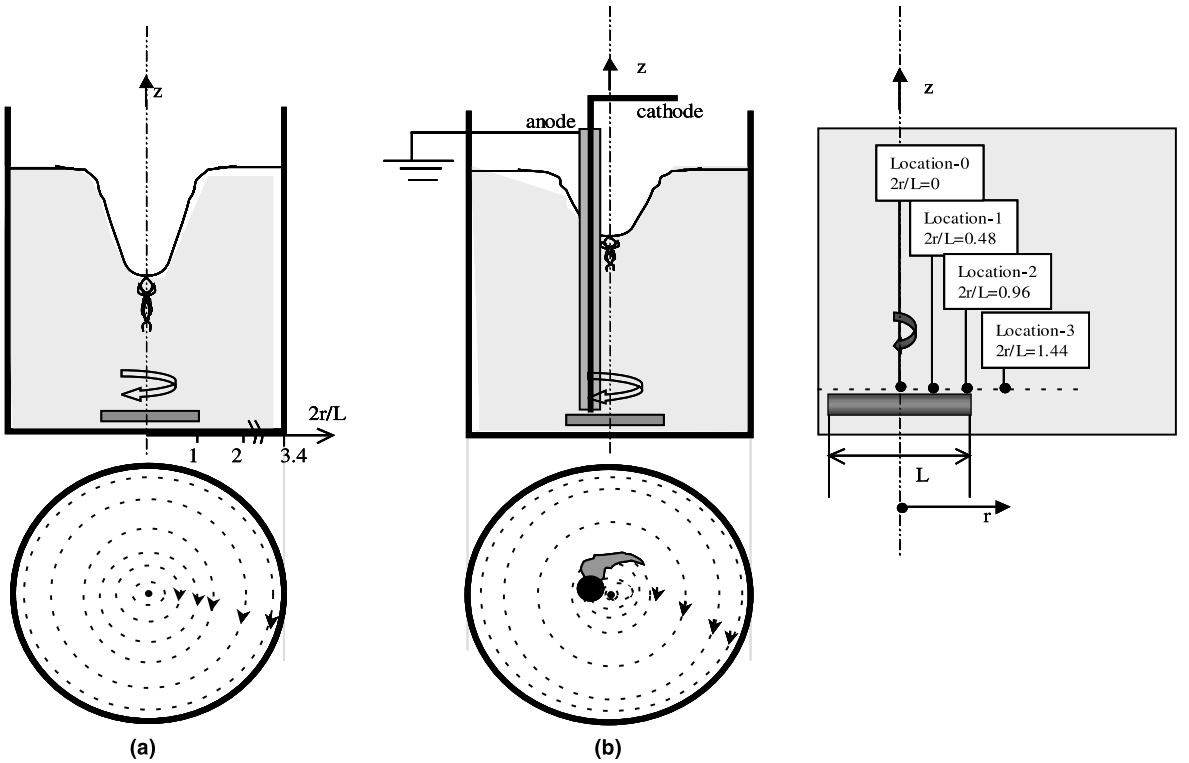

Fig. 1. Laser visualization sketches: (a) tank without probe; (b) flow past the probe; three-dimensional wake downstream the cylinder.

2.2. Flow visualization

The laser visualization was carried out in the flow without the electrochemical probe (a), and with the probe submerged in the flow (b). The results are sketched in Fig. 1. Rotation of the magnetic rod induces three-dimensional eddies. These eddies are modified by the probe to create complex vortex structures. The capability for the electrochemical diagnostics to detect these vortices, is one of the goal of the present study.

Without the probe (Fig. 1(a)) a central depression develops on the free surface and a vertical vortex line oscillates at its tail-end. The depth of the depression zone increases with the rotation rate Ω.

In the presence of the probe, the central depression decreases (Fig. 1(b)) and the vertical vortex line becomes less visible. Streamlines in a z-plane are weakly disturbed, particularly in the central region. Seeding particles tend to accumulate at the central core. Downstream the probe, streamlines are disturbed as Von Karmàn eddies shed in the vertical plane.

LDV was used to measure simultaneously the vertical and the tangential velocity components (Fig. 2). In the local cylindrical co-ordinates (r,θ,z), the vertical z-axis coincides with the axis of the reactor. The tangential (azimuthal) velocity component (V) is negative when the flow crosses the vertical measurement (r,z)-plane in clock-wise direction. The vertical component (W) is negative in downward direction. The profiles shown in Fig. 2 correspond to the location 1 for two cases: with the probe submerged or not. The tangential velocity profile V is linear for small r in the core of the flow. Beyond a maximum value, the V-component decreases as $(1/r)$. These flow characteristics can be associated with a rigid body rotation of the flow core. So, the main flow may be considered as a tornado wise flow which is axially pumped downwards by the stirrer and impinges at the bottom of the reactor. The liquid moves axisymmetrically towards the tank wall and is recycled up along the wall. In this region the vertical velocity component W becomes positive (Fig. 2). The velocity field is obviously disturbed when the electrode probe is submerged in the flow; for example the azimuthal velocity is very reduced.

3. Results and discussions

3.1. Time-averaged parameters

The influence of hydrodynamics on the time-averaged mass transfer values is presented in Table 1. The mean current $\bar{I}$ allows one to obtain the mean mass

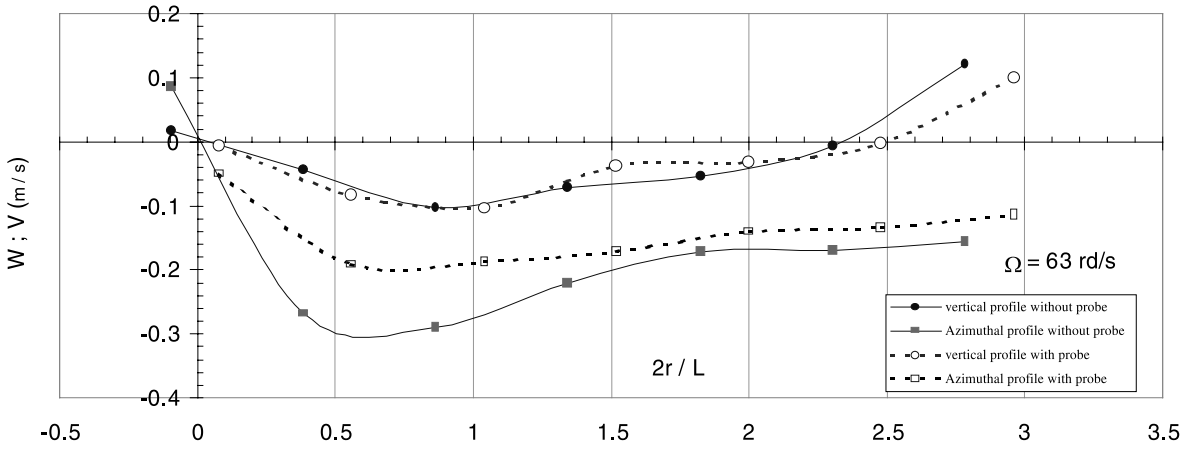

Fig. 2. Influence of the probe on the velocity profiles at the location 1. Vertical (W) and azimuthal (V) velocity components. Angular rate of the magnetic rod $\Omega = 63$ rad s^{-1}. Measurement stations lay on a radius tangent to the probe cylinder in the $z_0/b \sim 0.3$ plane.

transfer rate $\overline{K}$ on the electrode and the corresponding Sherwood number Sh and to evaluate the Nernst diffusion layer thickness δ_N:

$$\overline{K} = \frac{\bar{I}/A}{nFC_\infty}, \quad Sh = \bar{K}d/\mathscr{D}, \quad \delta_N = \mathscr{D}/\bar{K}. \tag{1}$$

In these relations, d is the cathode diameter and $\mathscr{D}$ is the molecular diffusion coefficient.

As expected, the diffusion layer thickness δ_N decreases when the rotation rate Ω increases, while the values of $\overline{K}$ vary inversely. For a given angular rate, the mass transfer rate $\overline{K}$ takes a maximum value for the locations 1 and 2. So does the Sherwood number. This maximum value is about 1.3 times the rate obtained near the axis (location 0) and at $2r/L \sim 1.44$ (location 4).

The measurements of the turbulence intensity $\sqrt{\overline{I'^2}}/\bar{I}$ related to the fluctuations of the limiting diffusion current give the values between 0.11 and 0.20. These values are larger than 0.10 commonly retained for two-dimensional flows [6]. These results may be explained by the influence of large eddies generated ever by the magnetic rod or the Karman vortices. These eddies reach the electrode surface and give rise to the strong fluctuations of the limiting diffusion current. In presence of large flow perturbations, the interpretation of mass transfer measurements by means of the well-known Levêque's equation $\bar{I} \sim \overline{\tau}^{1/3}$ may be questionable. Nevertheless, in Table 1 we just use Levêque's equation as a guide reference for estimation of the mean wall shear stress $\overline{\tau}$ and the associated parameters (friction length y_τ and friction velocity u_τ). The turbulence intensity $\sqrt{\overline{\tau'^2}}/\overline{\tau}$ concerning the fluctuations of the wall shear stress may then be evaluated from the measurements of $\sqrt{\overline{I'^2}}/\bar{I}$ by a linear approximation of the Levêque equation: $\sqrt{\overline{\tau'^2}}/\overline{\tau} \approx 3\sqrt{\overline{I'^2}}/\bar{I}$. The values of turbulence intensity which where obtained in our experiments at the location 1 and at the location 2 are surprisingly very close to the results reported by Mao and Hanratty [7,8] in the flow under sinusoidal oscillations.

3.2. Energy input: resonance peaks

The fluctuations of the limiting diffusion current at the location 2 are depicted in Fig. 3. These results correspond to flow excitation by the magnetic rod with the rotation frequency $\Omega \approx 67$ rad s^{-1}. A large number of oscillations is obtained. The PSD of the limiting diffusion current fluctuations confirms indeed the existence of many frequency peaks (Fig. 4). The resonance response of the diffusion layer to the hydrodynamical excitation is clearly shown by the most intense peak at $f = f_{res}$. The dependence of the resonance frequency of the diffusion layer on the hydrodynamical excitation frequency is represented in Table 2. It can be noted that at the location 1 ($2r_1/L = 0.48$) the resonance peak f_{res} coincides with the excitation frequency Ω. At the location 2 near the tip of the rod ($2r_2/L = 0.96$), the resonance frequency is equal to $\Omega/2$ for $\Omega = 63$ and 82 Hz. These results tend to prove that:

(i) Coherent hydrodynamical structures generated by the stirrer in the bulk of the flow reach the near electrode region and excite the diffusion layer. As the result, the resonance peaks appear in the power spectrum density (PSD) of the current fluctuations.
(ii) Excitation frequency of the coherent hydrodynamical structures is correlated to the rotation frequency of the mechanical device. Depending on the diffusion layer conditions, the resonance in the mass transfer rate occurs either on the excitation frequency or on its sub-harmonics.

Table 1
Order of magnitude of the mean values of variables

Non-dimensional location, $2r_i/L$	Angular rate, $\Omega = 2\pi N$ (rad s^{-1})	Mass transfer coefficient, $\overline{K}$ (m s^{-1})	Sherwood number, Sh	Nernst layer, δ-Nernst (m)	Fluctuation rate of current intensity, $\sqrt{i^2}/\overline{I}$	Wall friction, τ (N m^{-2})	Friction velocity, u_τ (m s^{-1})	Dimensional y-co-ordinate scale $y_\tau = \nu/u_\tau$ (m)	Non-dimensional electrode diameter $d^+ = d/y_\tau$
0 (axis)	37	7.08E − 05	48.16	1.04E − 05	0.20	0.51	0.023	4.41E − 05	11.32
	63	9.99E − 05	67.99	7.35E − 06	0.19	1.44	0.038	2.63E − 05	18.99
	82	1.15E − 04	78.03	6.41E − 06	0.19	2.18	0.047	2.14E − 05	23.35
Location 1, 0.48	37	9.48E − 05	64.48	7.75E − 06	0.13	1.23	0.035	2.85E − 05	17.54
	63	1.30E − 04	88.1	5.68E − 06	0.13	3.14	0.056	1.78E − 05	28.02
	82	1.43E − 04	97.15	5.15E − 06	0.13	4.21	0.065	1.54E − 05	32.44
Location 1, 0.96	37	9.05E − 05	61.54	8.13E − 06	0.11	1.07	0.033	3.06E − 05	16.35
	63	1.35E − 04	91.98	5.44E − 06	0.12	3.57	0.06	1.67E − 05	29.88
	82	1.49E − 04	101.46	4.93E − 06	0.12	4.79	0.069	1.44E − 05	34.62
Location 3, 1.44	37	7.07E − 05	48.11	1.04E − 05	0.17	5.11	0.023	4.42E − 05	11.3
	63	1.04E − 04	70.66	7.08E − 06	0.16	1.62	0.04	2.48E − 05	20.12
	82	1.19E − 04	80.71	6.20E − 06	0.15	2.41	0.049	2.04E − 05	24.56

3.3. Energy repartition: analysis of the PSD and identification of the peaks

Many resonance frequencies can be observed when plotting the PSD against the frequency co-ordinate for the location 1 (Fig. 5). Such a situation may depict some superimposed mechanisms. Taking the resonance frequency f_1 (f_1 stands for f_{res}) as a reference, we have succeeded to identify in this spectrum the existence of the frequencies $1/2f_1, 1/4f_1, \ldots$, which represent its sub-harmonics. The existence of the odd harmonics of each of these frequencies is clearly noticeable: $3f_1/2, 5f_1/2, \ldots$ and $3f_1/4, 5f_1/4, 7f_1/4$. These frequencies may correspond to a non-linear sub-harmonic mechanism. Besides, a second frequency $f_2 = 6.25$ Hz, which does not fit in the former mechanism, can be detected. This frequency is independent from f_1 and can be induced by the secondary flow past the probe, but further investigations should be provided to confirm this hypothesis. Thus, we deal with a two-frequency process. Many frequencies involving f_2 are detected: $f_1 \pm f_2, 2f_1 \pm f_2, 1/2$ $f_1 \pm f_2, 3/\ 2f_1 \pm f_2, \ldots$ They are supplied by a non-linear interaction mechanism. These interconnected mechanisms generate period doublings and make the signal definitely more complex. The results at location 2 lead to the similar conclusion.

In addition, Fig. 5 indicates an exponential damping of the energy base line. Davoust et al. [10] have reported a similar behavior in magneto-hydrodynamic flows. According to the authors [10,11], the exponential damping mechanism is strongly controlled by the aspect ratio of the system. Exponential damping (or increase) rates of instabilities are rather commonly reported in linear theories for transition to turbulence.

3.4. Influence of the rotation rate and of the probe location

For a given location, the peaks progressively disappear from the PSD curve of the current fluctuations when Ω varies from 37 to 82 rad s^{-1}, Fig. 6. In the meanwhile the base line of PSD increases significantly as Ω is increased. Only the excitation peak and its first sub-harmonic remain significant. This behavior is typical for the development of flow turbulence [9].

When the probe is moved from the location 1 to the location 3 without changing the rate of mechanical excitation, a complete disappearance of the sub-harmonics $f_1/4$ and its odd harmonics is noticed. The same phenomenon occurs for some other peaks resulting from the interaction between f_1 and f_2. The remaining peaks spread out. We can conclude that at the location 3, almost all the frequencies are absorbed by the base line. Only the frequency peak f_2 remains significant at the location 3. This shows that the frequency f_2 is independent from the phenomenon related to the frequency

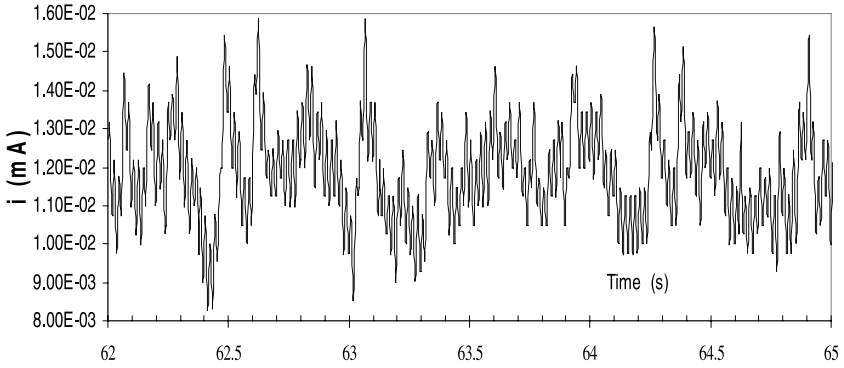

Fig. 3. Limiting diffusion current fluctuations at the location 2. Angular rate $\Omega = 67$ rad s^{-1}.

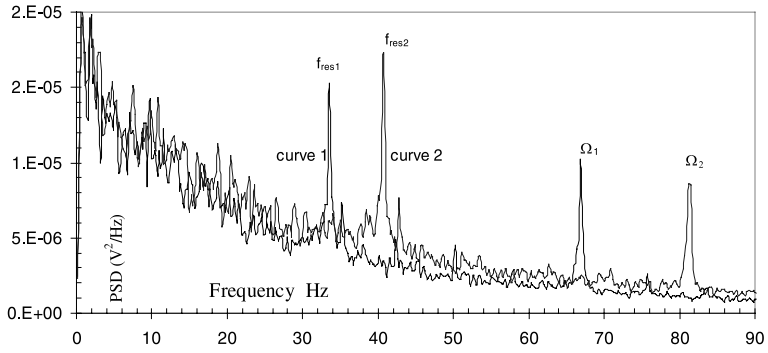

Fig. 4. PSD of the limiting diffusion current signal at location 2. Resonance frequencies. Angular rate $\Omega = 67$ rad s^{-1} (curve 1); $\Omega = 82$ rad s^{-1} (curve 2).

f_1 (vortex generated by the stirrer). This is an additional confirmation that the frequency f_2 is related to the secondary flow generated by the probe.

The re-organization of the flow is very important from one location to the other. At the locations 1 and 2 the working electrode is very close to the stirrer and the influence of the coherent structures on mass transfer is important. At the location 3 the distance between the working electrode and the stirrer is about the stirrer length, only. But it is enough for an important development of the turbulence which results in "stochastic" characters of the PSD-curves. These conclusions are similar to the results of Michelet et al. [1]. These authors have investigated the variation of the macro-length scale (L_Δ). The macro-length represents the length over which the coherent structures persist. The parameter L_Δ was calculated at different stations along an axis Δ tangent to the turbine disc. According to their results [1], L_Δ increases until a dimensionless parameter, equivalent to $2r/d_0$ in the present paper, reaches 0.7. Then L_Δ rapidly decreases. That is also in agreement with the investigations of Wu et al. [4] who found that the periodic fluctuations dominate the turbulence field close to the impeller in an agitated tank, but rapidly diminish away from the tip region. At $2r/L \sim 1.5$, the authors found that the periodic structures are reduced to about 20% of the total energy of the fluctuations. This phenomenon characterizes the development of the bulk turbulence.

Table 2
Resonance frequencies

Location 1, $2r_1/L = 0.48$, $f_{res} \sim \Omega$		Location 2, $2r_2/L = 0.96$, $f_{res} \sim 0.5\Omega$	
Excitation Ω (Hz)	Resonance f_{res} (Hz)	Excitation Ω (Hz)	Resonance f_{res} (Hz)
37	35.4	37	17.7 (or 35.2 ?)
63	67.0	63	33.6
82	81.4	82	40.6

3.5. Similarity of the energy repartition

In the paragraph 3.2 it was noted that the input of the mechanical energy to the system could be related to the onset of a resonance peak f_{res}. PSD curves obtained for different excitation frequencies Ω show some similarity in the energy distribution. For example, in Fig. 7,

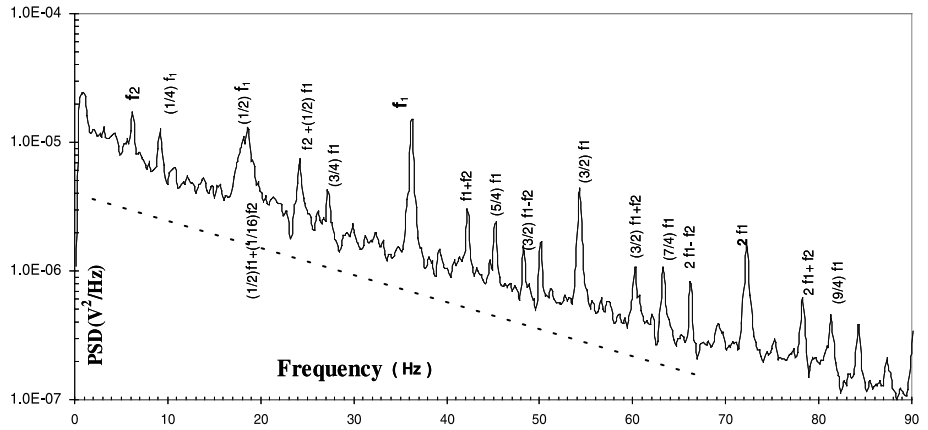

Fig. 5. PSD of the limiting diffusion current signal at location 1. Sub-harmonics cascade and non-linear interactions. Angular rate $\Omega = 67$ rad s^{-1}.

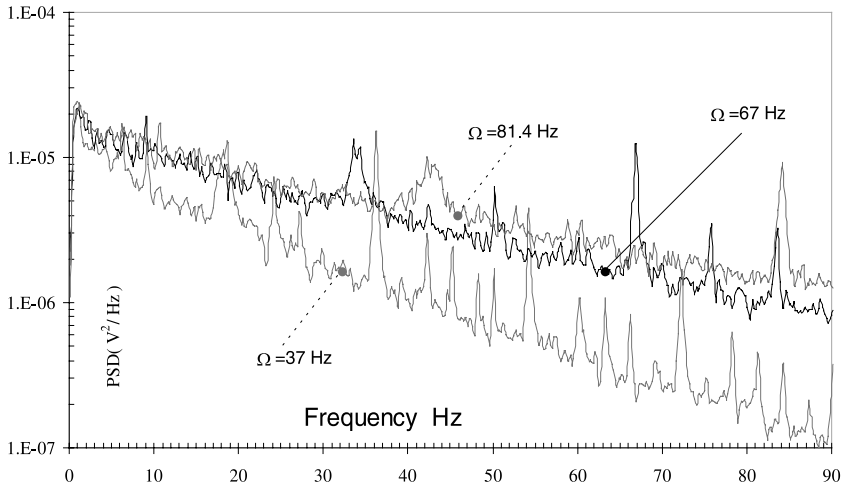

Fig. 6. Development of turbulence by increasing the rotation rate at the location 1.

the PSD curves are plotted against the dimensionless frequency f/f_{res} for different Ω at the location 1. One can see that all these curves coincide. A cut-off point is obtained at $(f/f_{\text{res}})_1 \approx 3$. The same similarity in the energy repartition is obtained for the location 2. For this latter case, the cut-off point is obtained at $(f/f_{\text{res}})_2 \approx 6$.

Previously, we have obtained (Table 2) that the resonance frequencies are: $(f_{\text{res}})_1 = \Omega$ and $(f_{\text{res}})_2 = \Omega/2$. So, for both locations a critical cut-off frequency is given by the ratio $f/\Omega \approx 3$. Therefore it is worthy to plot PSD against f/Ω co-ordinate. The resulting similarity in the energy repartition is given in Fig. 8 corresponding to the two locations. A change in the damping of the energy can be noticed for critical frequency $f/\Omega \approx 3$. The exponential damping described in Section 3.3 is valid in the range $0.5 \leqslant f/\Omega \leqslant 3$. For higher frequency range $(f/\Omega > 3)$, the energy damping seems to be governed by an asymptotic power law: $[f/\Omega]^m$, where $m \approx -3$ (Fig. 8). The same asymptotic law was reported in [15]. In this reference, the PSD of the limiting diffusion current was obtained in electrochemical cell with complex geometry agitated by an impeller.

4. Conclusions

Limiting diffusion current measurements were carried out in a small tank, agitated by a magnetic rod. The configuration with a submerged cylinder as a counter electrode, containing the small working electrode, was used. Mass transfer on the working electrode and flow structure in the vicinity of the stagnation region was studied.

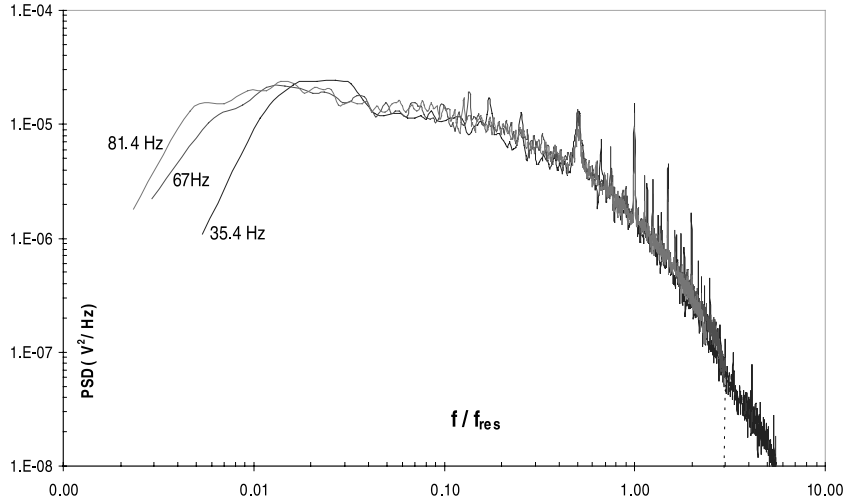

Fig. 7. Similarity of the energy repartition at the location 1. Resonance frequencies are 35.4, 67 and 81.4 Hz, respectively.

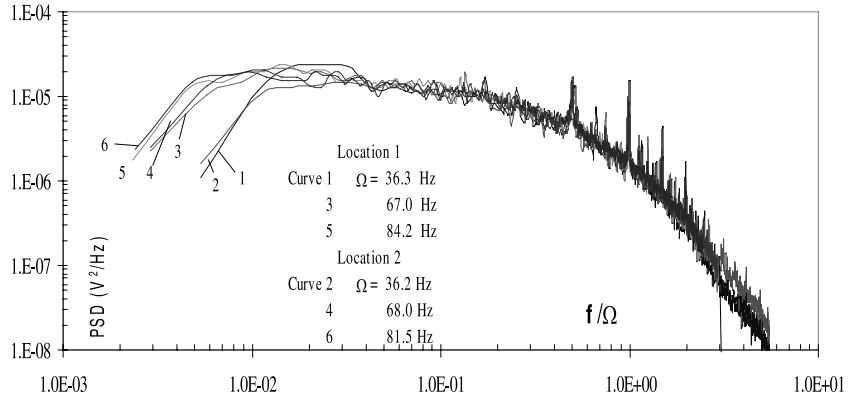

Fig. 8. Overall similarity of the energy repartition at the locations 1 and 2.

The PSD analysis of the fluctuations of the limiting diffusion current reveals the existence of resonance peaks. These peaks are related to the influence of large eddies generated by the stirrer. Indeed, for a given location of the probe, the most important resonant peak f_{res} coincides either with the agitator's rate (it means with mechanical excitation frequency Ω) or with its sub-harmonics $\Omega/2$. It was also noted the existence of another resonance frequency f_2 independent from Ω and from the probe position. It seems that this frequency is related to the secondary flow past the cylinder. So, the electrochemical measurements are sensitive to detect by means of PSD analysis the coherent structures arising in complex 3D turbulent flows.

The use of PSD analysis allows to describe some mechanisms of development of turbulence in the agitated tank:

- A sub-harmonic cascade, down to at least $1/4f_{res}$, is detected in the spectrum when the probe locations are chosen in the very vicinity of the magnetic rod. Odd harmonics of resonant frequency are also detected.
- The observed peaks disappear quickly when the probe is moved away from the excitation source. The peaks also disappear when the rotation rate is increased. That proves a rather fast development of the turbulence in agitated tank.
- Independent frequencies, f_1 and f_2, generate non-linear interaction frequencies $n_1f_1 \pm n_2f_2$ which fill up the spectrum.

It is shown that a similarity in the energy repartition exists if PSD is presented with respect to f/Ω co-ordinate. A non-dimensional frequency cut-off appears at

$f/\Omega \approx 3$. In the low frequency range, $0.05 < f/\Omega \leqslant 3$, the spectra are found to verify an exponential damping law. For higher frequency range, $f/\Omega > 3$, the energy damping seems to be governed by a asymptotic power law $[f/\Omega]^m$, where $m \approx -3$.

References

[1] S. Michelet, A. Kemoun, J. Mallet, M. Mahouast, Space-time velocity correlations in the impeller stream of a Rushton turbine, Exp. Fluids 23 (1997) 418–426.

[2] K. Ogawa, Y. Mori, Size effect on spectrum of turbulent energy in a stirred vessel, J. Chem. Eng. Jpn. 30 (5) (1997) 969–971.

[3] H. Wu, G.K. Patterson, M. Van Doorn, Distribution of turbulence energy dissipation rates in a Rushton turbine stirred mixer, Exp. Fluids 8 (1989) 153–160.

[4] H. Wu, G.K. Patterson, Laser Doppler measurements of turbulent flow parameters in a stirred mixer, Chem. Eng. Sci. 44 (10) (1989) 2207–2221.

[5] E.S. Wernersson, C. Trägardh, Turbulence characteristics in turbine agitated tanks of different sizes and geometries, Chem. Eng. J. 72 (1999) 97–107.

[6] T.J. Hanratty, J.A. Campbell, Measurement of wall shear stress, in: R.J. Goldstein (Ed.), Fluid Mechanics Measurements, Hemisphere, Washington, 1983, pp. 559–615.

[7] Z.X. Mao, T.J. Hanratty, Influence of large amplitude sinusoidal and non-sinusoidal oscillations on drag, in: Proceedings of 3rd International Workshop on Electrodiffusion Diagnostics of Flows, Dourdan, 1993, pp. 119–128.

[8] Z.X. Mao, T.J. Hanratty, Application of an inverse mass transfer method to the measurement of turbulent fluctuations in the velocity gradient at the wall, Exp. Fluids 11 (1991) 65–73.

[9] P. Bergé, Y. Pomeau, C. Vidal, L'ordre dans le chaos, in: Vers une approche déterministe de la turbulence, Hermann, Editeurs des sciences et des arts, Paris, 1988, pp. 226–233 (Chapter 8).

[10] L. Davoust, R. Moreau, R. Bolcato, Roads to turbulence for an internal MHD buoyancy-driven flow due to a horizontal temperature gradient, in: Alemany et al. (Eds.), Transfer Phenomena in Magnetohydrodynamics and Electroconducting Flows, 1999, pp. 127–133.

[11] P. Manneville, Chaos et structures dissipatives, Collection Aléa-Saclay, 1991, pp. 114–117.

[12] H.B. Oldham, J.C. Myland, Fundamentals of Electrochemical Science, Academic Press, New York, 1994.

[13] V.G. Levich, Physicochemical Hydrodynamics, Prentice-Hall, Englewood Cliffs, NJ, 1962.

[14] S.A. Martemyanov, T.N. Khomchenko, L.N. Nekrasov, B.M. Grafov, Possibility of using electrolyte turbulent pulsations to study electrochemical reactions kinetics, Electrokhimiya 26 (4) (1990) 498–500, English translation, Sov. Electrochem. 26 (4) (1990).

[15] T.N. Khomchenko, S.A. Martemyanov, L.A. Sokolov, L.N. Nekrasov, B.M. Grafov, Spectral characteristics of turbulent diffusion layer under chaotic electrolyte stirring conditions, Electrokhimiya 25 (11) (1989) 1546–1548, English translation, Sov. Electrochem. 25 (11) (1989) 1384–1389.

[16] T.N. Khomchenko, L.N. Nekrasov, X. Almualla, S.A. Martemyanov, B.M. Grafov, Spectrum of turbulent pulsations of electrochemical current under conditions of formation of low-soluble reaction products, Electrokhimiya 33 (1) (1997) 31–35, English translation, Russ. J. Electrochem. 33 (1997).